Article

A New Supported Manganese-Based Coordination Complex as a Nano-Catalyst for the Synthesis of Indazolophthalazinetriones and Investigation of Its Antibacterial Activity

Maryam Ariannezhad [1],* , Davood Habibi [1], Somayyeh Heydari [1,2] and Vahideh Khorramabadi [1]

[1]   Department of Organic Chemistry, Faculty of Chemistry, Bu-Ali Sina University, Hamedan 6517838683, Iran; davood.habibi@gmail.com (D.H.); somi.heydari@gmail.com (S.H.); vahide.khoram@yahoo.com (V.K.)
[2]   Department of Research and Development of the Faran Shimi Pharmaceutical Company, Tuyserkan 6586166833, Iran
*   Correspondence: mary.ariannezhad@yahoo.com

Abstract: A new magnetic supported manganese-based coordination complex (Fe_3O_4@SiO_2@CPTMS @MBOL@ Mn) was prepared in consecutive stages and characterized via various techniques (VSM, SEM, TEM, XRD, FT-IR, EDX, TG-DTA, and ICP). To evaluate its application, it was used for synthesis of divers Indazolophthalazinetriones in a simple procedure via the one-pot three-component condensation reaction of aldehydes, dimedone, and phthalhydrazide in ethanol under reflux conditions. The Mn catalyst can be recycled without any noticeable loss in catalytic activity. Additionally, the antibacterial properties of the nano-catalyst were studied against some bacterial strains.

Keywords: aldehyde; dimedone; indazolophthalazinetrione; phthalhydrazide; Mn-supported nano-catalyst

1. Introduction

Phthalazine derivatives have an important role in heterocyclic compounds that have received terrific interest in the field of pharmaceuticals and biological activities and led to clinical applications [1] such as antifungal [2], anti-inflammatory [3], anticonvulsant [4], anticancer [5], and cardiotonic [6]. In addition, these compounds represent specific optical properties [7]. Multi-component reactions (MCRs) are remarkable mechanisms for preparation of a wide variety of organic compounds via better efficiency in one step with at least three or more starting materials [8]. Applying a large number of different types of catalyst which accelerate and proceed the reaction in smooth conditions has been extensively developed for this specific issue [9–11]. Several synthetic methodologies have been reported for the synthesis of phthalazine derivatives such as one-pot three or four component condensation reactions [12–16]. For example, Fe_3O_4@Cys-SO_3H was used by Kefayati and coworkers as a catalyst for the synthesis of 2*H*-indazolo[2,1-*b*]phthalazinetriones derivatives in ethanol under reflux conditions [17]. Shirini and coworkers prepared [PVPH]ClO_4 as an efficient and reusable solid acid polymeric catalyst for the synthesis of 2*H*-indazolo[2,1-*b*]phthalazine triones in the same way as using initial reagents through the one-pot reaction at 100 °C in solvent-free conditions [18]. Heirati team investigated the implementation of O-sulfonic acid poly(4-vinylpyrrolidonium) chloride as an effective catalyst for the same synthesis at 80 °C in solvent-free conditions [19]. Rostamnia and coworkers synthesized a series of mentioned products with similar reagents using the Fe_3O_4@GO-Pr-SO_3H catalyst in ethanol [20]. 5-sulphosalicylic acid was used by Karhale and coworkers as an organocatalyst for the one-pot synthesis of Indazolophthalazinetriones from the previous substrates [21]. Varghese and coworkers, through a significant method, produced them

with similar reagents in the presence of iodine under ultrasonic irradiation [22]. Mosad-degh's group succeeded in synthesizing phthalazinetriones derivatives through a rapid, one-pot, four-component route by using Ce(SO$_4$)$_2$4H$_2$O at 125 °C and under solvent-free conditions [23]. However, some methods experienced some limitations such as tedious workup procedures, using corrosive catalysts, low product yields, long reaction times, formation of side products, and difficulties in recovery of catalysts [24].

Due to concerns about environmental issues, different strategies were applied to reduce the side-effects of chemical industries. For instance, using solvent-free techniques, eco-friendly materials, ultrasound or microwave methods, and finally, recyclable catalysts [25]. In recent years, the application of magnetic nanoparticles (MNPs) according to the super magnetic property and facile separation from reactions media, high surface area, low toxicity, biocompatibility, good stability, and low-cost option has obtained notice-able regards for chemists using catalysts in chemical reactions. Moreover, MNPs can be functionalized completely via proper surface modifications. Based on the mentioned prop-erties, many MNPs-supported catalysts have been effectively applied to improve a large number of chemical reactions [26,27]. Among the heterogeneous catalysts, the magnetic supported metal complexes have a special place [28]. Thereby, we would like to announce the synthesis of a novel Mn-supported nano-catalyst (Fe$_3$O$_4$@SiO$_2$@CPTMS@MBOL@Mn) in consecutive stages (Scheme 1).
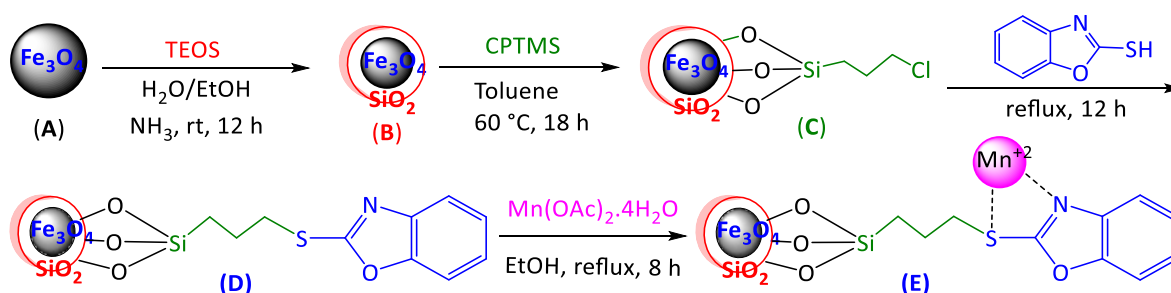
Scheme 1. Synthesis of a novel Mn-supported nano-catalyst. (**A**) Fe$_3$O$_4$·MNPs, (**B**) Fe$_3$O$_4$@SiO$_2$, (**C**) Fe$_3$O$_4$@SiO$_2$@ CPTMS, (**D**) Fe$_3$O$_4$@SiO$_2$@CPTMS@MBOL, and (**E**) Fe$_3$O$_4$@SiO$_2$@CPTMS@MBOL@Mn.

Then, the Mn nano-catalyst was characterized by various techniques (VSM, SEM, TEM, XRD, FT-IR, EDX, TG-DTA, and ICP) and used for the synthesis of diverse Indazoloph-thalazinetriones in an efficient procedure via the one pot three-component condensation reaction of aldehydes, dimedone, and phthalhydrazide in ethanol under reflux conditions (Scheme 2).
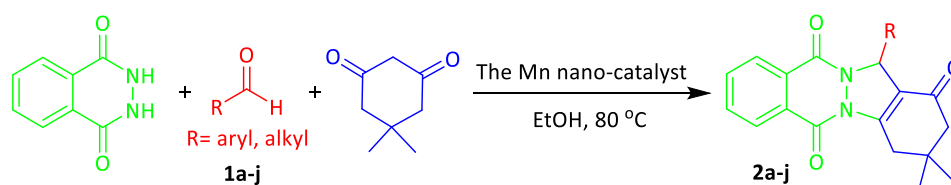
Scheme 2. Synthesis of diverse indazolophthalazinetriones.

2. Results and Discussion

2.1. Characterization

2.1.1. ICP Analysis of the Mn-Supported Nano-Catalyst

The Mn content of the nano-catalyst was about 0.27% according to ICP analysis.

2.1.2. FT-IR Spectroscopy of the Mn-Supported Nano-Catalyst

Figure 1 illustrates the FT-IR spectra for each step of preparation of nano-catalyst that includes (**A**) Fe$_3$O$_4$·MNPs, (**B**) Fe$_3$O$_4$@SiO$_2$, (**C**) Fe$_3$O$_4$@SiO$_2$@ CPTMS, (**D**) Fe$_3$O$_4$@SiO$_2$@CPTMS@MBOL, and (**E**) Fe$_3$O$_4$@SiO$_2$@CPTMS@MBOL@Mn. In part **A**, the existence of

stretching vibrations peak for Fe-O is characteristic at about 578 cm^{-1}. The appearance of a wide peak close to 1087 cm^{-1} in part **B** indicates the coating of silica with magnetite nanoparticles. Part **C** exhibits a unique peak at about 583 cm^{-1}, confirming the presence of the C-Cl bond. Part **D** shows two newly discovered peaks at 1345 and 1664 cm^{-1} which are corresponded to the C-N and C=N bonds, respectively. Part **E** indicates a shift from 1664 to 1602 cm^{-1} which could be in accordance with the new interaction of manganese with the nitrogen of the C=N bond. In addition, at 408.93 cm^{-1}, a weak peak appeared, corresponding to the Mn-N band. Therefore, the comparison of all the IR spectra approved the successful formation of the Mn-supported nano-catalyst.
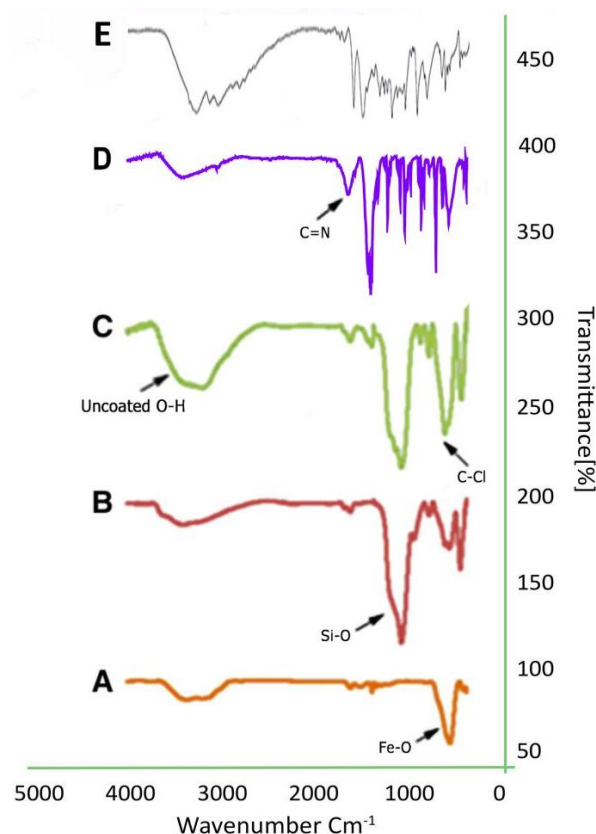

Figure 1. FT-IR spectra of five steps of preparation of the nano-catalyst (**A**–**E**).

2.1.3. XRD Analysis of the Mn-Supported Nano-Catalyst

In order to evaluate the crystallographic structure of Fe_3O_4@SiO_2@CPTMS@MBOL@Mn, XRD analysis was carried out for Fe_3O_4@SiO_2 (grey), Fe_3O_4@SiO_2@CPTMS (red), Fe_3O_4@SiO_2@CPTMS@MBOL (blue), and Fe_3O_4@SiO_2@CPTMS@MBOL@Mn (green) and is shown in Figure 2. The diffraction peaks at 2θ = at 10, 30, 35, 45, 53, 57, and 63 (JCPDS 19-0629) [29] approve the silica effectively coated on the cubic spinel crystal planes of Fe_3O_4. The XRD pattern of Fe_3O_4@SiO_2@CPTMS@MBOL@Mn [29,30] indicates the crystalline nature of the nano-catalyst at 2θ = 30, 35, 39, 43, 56 which responded to the Mn catalyst (JCPDS 24-0508) [31]. Through Debye-Scherrer formula, the obtained particle size was about 34.68 nm. In fact, due to the reduction of intensity, the core-shell structure could be anticipated, and the Fe_3O_4·MNPs particles were coated with ligand profitably [32–34].
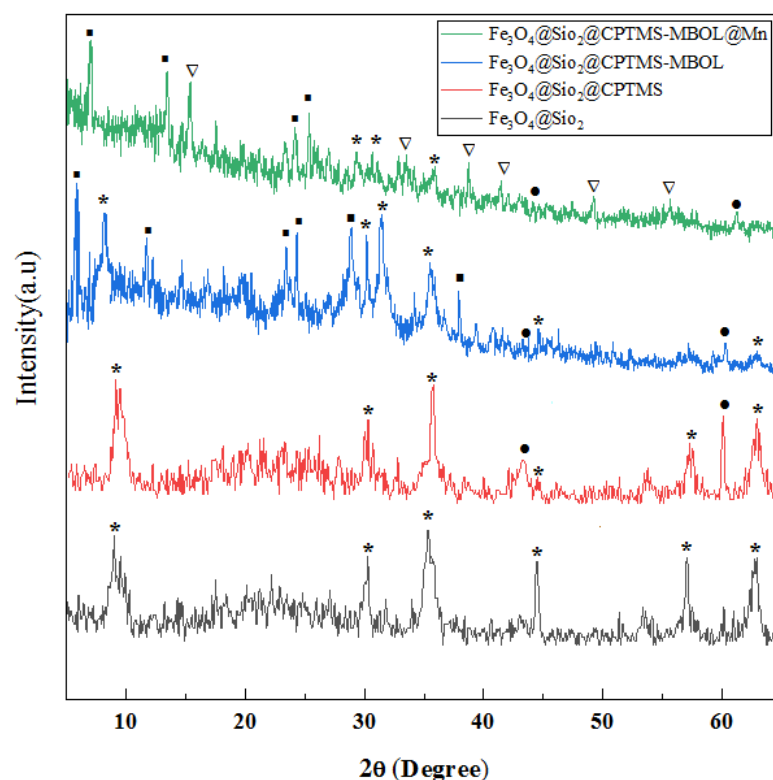
Figure 2. The XRD pattern of $Fe_3O_4@SiO_2@CPTMS@MBOL@Mn$.

2.1.4. EDX Analysis of the Mn-Supported Nano-Catalyst

The elemental structure of the Mn-supported nano-catalyst was disclosed by EDX analysis (Figure 3). The results ratified the existence of the predictable elements in the construction of the catalyst, including C, N, O, Si, S, Fe, and Mn. Generally, the samples were coated with a very thin layer of gold that led to appearance of the Au peak in the EDX graph analysis as well.
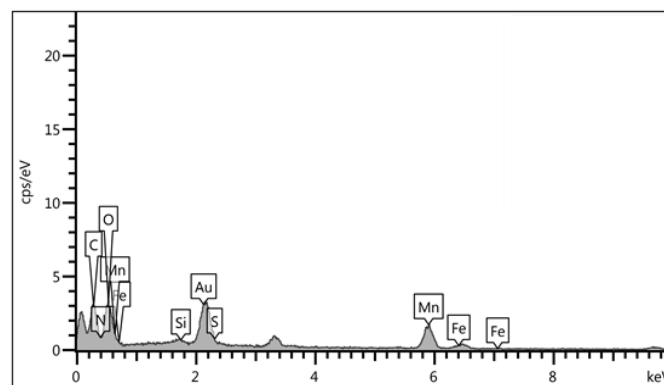
Figure 3. EDX analysis of the Mn-supported nano-catalyst.

2.1.5. SEM and TEM Analysis of the Mn-Supported Nano-Catalyst

In another evaluation, the morphology and size of the Mn-supported nano-catalyst were determined by SEM and TEM images (Figures 4 and 5). The spherical shape of the $Fe_3O_4@SiO_2@CPTMS@MBOL@Mn$ was conceived through the uniform nanometer-sized particles. In the SEM images, the formation of sintered grains within the 35–47 nm size range was apparent. The core–shell structure of nano-catalyst can be observed via TEM images. However, magnetostatic interactions of the particles could be the reason of some particle aggregations. At an exact scrutiny, according to distribution histograms (Figure 6), the average particle size for the nanoparticles was distributed between 19.1 and 29.7 nm.

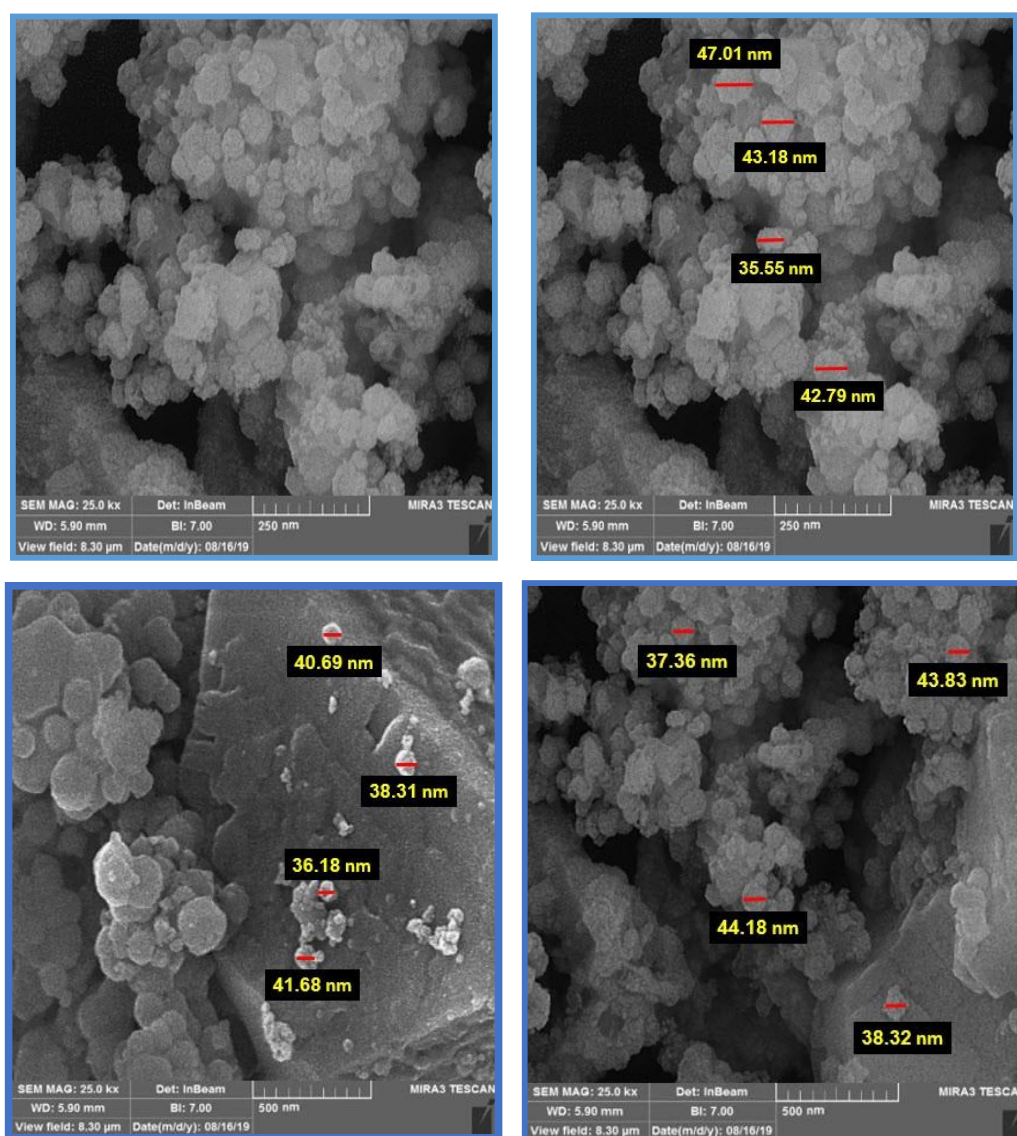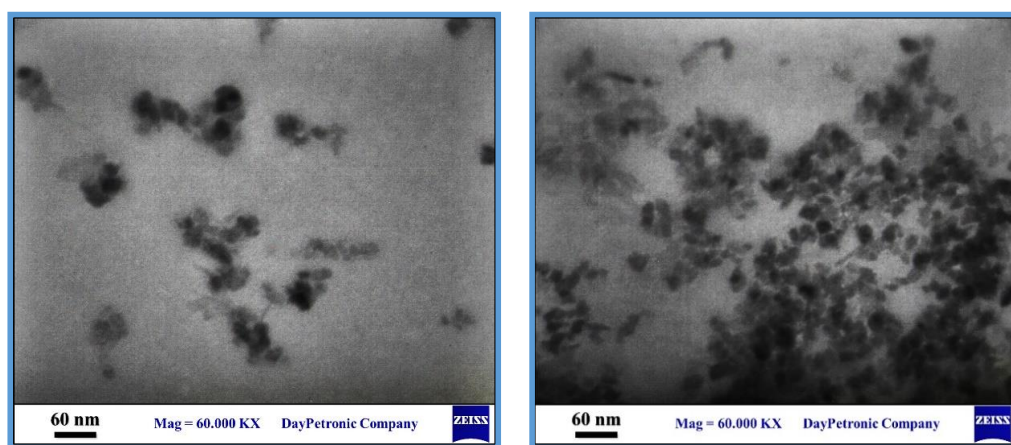**Figure 4.** SEM images of the Mn-supported nano-catalyst.

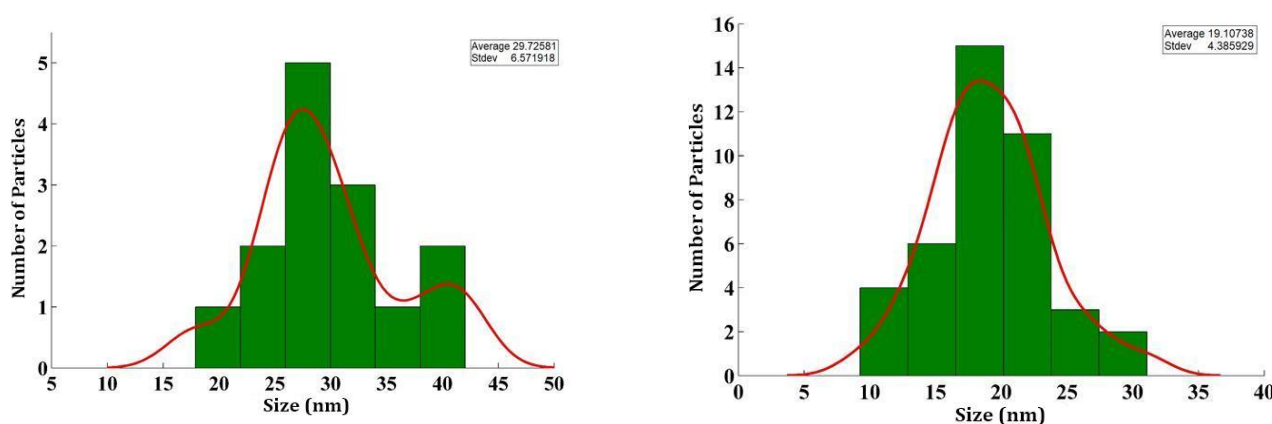**Figure 5.** TEM images of the Mn-supported nano-catalyst.

Figure 6. Particle size distribution of Mn catalyst.

2.1.6. Thermal Properties of the Mn-Supported Nano-Catalyst

Thermogravimetric analysis of the Mn nano-catalyst indicated the mass loss of the organic materials as they decomposed upon heating (Figure 7). As can be observed, there were about tree weight loss stages for the catalyst in the ranges of 100, 185, and 300 °C, respectively, in the temperature range of DTG analysis. In fact, DTG is a type of thermal analysis in which the rate of material weight changes upon heating is plotted against temperature and used to simplify the reading of weight versus temperature thermogram peaks which occur close together. The initial weight reduction at about 100 °C probably corresponded to the residual water, the second weight loss at about 180 °C was possibly attributed to the thermal decomposition of the complex, the third weight loss at about 300 °C was attributed to the thermal decomposition of the two CPTMS and MBOL ligands. As a result, reasonable thermal stability in accordance with coated layers on the surface of the support was approved, and it was shown that the nano-catalyst had a good strong interaction between the ligands and $Fe_3O_4 \cdot MNPs$ [35,36].

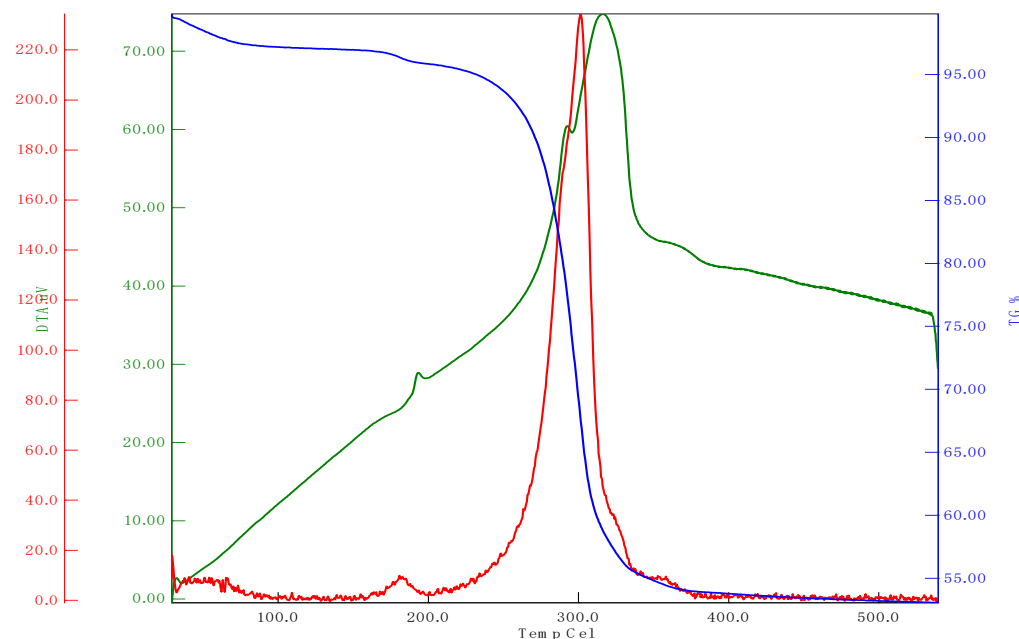**Figure 7.** TGA-DTA patterns of the Mn-supported nano-catalyst.

2.1.7. VSM Analysis of the Mn-Supported Nano-Catalyst

Due to the comparison of magnetic properties, VSM analysis was performed for (**A**) $Fe_3O_4 \cdot MNPs$, (**B**) $Fe_3O_4@SiO_2$, (**C**) $Fe_3O_4@SiO_2$-CPTMS, (**D**) $Fe_3O_4@SiO_2@CPTMS@MBOL$, and (**E**) $Fe_3O_4@SiO_2@CPTMS@MBOL@Mn$ (Figure 8). Generally, all five steps of forma-

tion showed magnetic possessions, and a clear decrease from **A** to **E** (65, 35, 30, 10, and 4.35 emu/g, respectively) could be observed. In fact, the dipolar-dipolar interactions were reduced between the magnetic nanoparticles due to coating of $Fe_3O_4 \cdot MNPs$ via different layers and complexation.
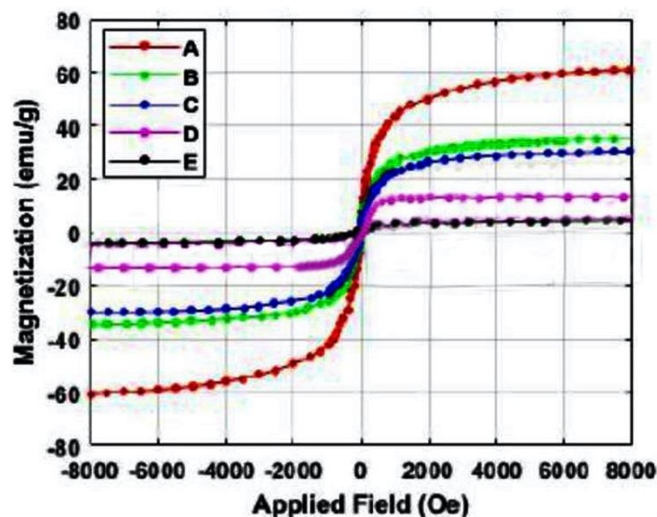

Figure 8. VSM analysis of **A**–**E**.

3. Experimental

3.1. General

All chemicals (starting materials, reagents, solvents, etc.) were acquired from the Merk (Berlin, Germany) and Aldrich (Darmstadt, Germany) companies and used in the absence of additional purification.

3.2. Preparation of the Mn-Supported Nano-Catalyst

The Mn-supported nano-catalyst was prepared according to the procedure described in [36]. Coprecipitation is an appropriate and low-cost procedure for the preparation of bare magnetite nanoparticles (MNPs). In order to prepare functionalized Fe_3O_4, $FeCl_3 6H_2O$ (11.44 g) and $FeCl_2 4H_2O$ (4.3 g) were dissolved in 100 mL distilled water and heated at 80 °C for 45 min. Then, 15 mL of aqueous ammonia (37%) was added dropwise to the mixture and heated for about 30 min at 80 °C. After separation by an external super magnet, the nanoparticles were washed 3 times with water and dried. Afterwards, MNPs (0.1 g) were added to a mixture of ethanol, distilled water (80 mL, 4:1 by volume), and aqueous ammonia (2 mL), and after dispersing under ultrasonic conditions for 10 min, 2 mL of Tetraethyl orthosilicate (TEOS) was slowly added, and the mixture was stirred for 6 h. The obtained solid from the previous step was added to the mixture of 1 mL 3-Chloropropyl(trimethoxy)silane (CPTMS) dissolving in anhydrous toluene (80 mL), and the mixture was put on the stirrer for 18 h at 60 °C. In the fourth stage due to functionalization, 2-mercapto-benzoxazole (MBOL, 0.75 g) as an organic ligand was added to the previous step product (0.1 g), and after addition of potassium carbonate (0.69 g, 5 mmol), the mixture in toluene (50 mL) was fixed under reflux conditions for 12 h. The solid was washed with toluene and water, respectively, and dried under reduced pressure. At the end, $Fe_3O_4@SiO_2@CPTMS@MBOL$ (0.1 g) was added to dispersed $Mn(OAC)_2 4H_2O$ (0.85 g, 5 mmole) in ethanol and stirred strongly for 10 h at reflux conditions. Then, the final product was separated with a strong magnet, washed with ethanol, and dried.

3.3. General Procedure for the Synthesis of Indazolophthalazinetriones

Phthalhydrazide (0.162 g, 1.0 mmole), dimedone (0.140 g, 1.0 mmole), an aldehyde derivative (1.0 mmole), and the Mn-supported nano-catalyst (20 mg) were mixed in ethanol (5 mL), stirred, and heated at reflux conditions for appropriate times, which depended on the substrate and completion of the reaction was monitored by TLC. After cooling, the Mn-supported nano-catalyst was separated by a super magnet, H_2O (10 mL) was added, and a white precipitate was filtered and recrystallized in EtOH.

3.4. Optimization

To obtain the best result, the effects of different conditions were investigated for this reaction. The one-pot three-component condensations of phthalhydrazide (1.0 mmole), 4-methylbenz-aldehyde (1.0 mmole), and dimedone (1.0 mmole) was chosen as a model reaction in different reaction conditions (amount of the catalyst, temperature, and solvent). The best result was achieved with 1.0 mmole of 1:1:1 of benzaldehyde/dimedone/phthalhydrazide in presence of 20 mg of the Mn-supported nano-catalyst in EtOH under reflux conditions (Table 1, entry 5).

Table 1. Optimization of the reaction conditions.

Entry	Solvent	Catalyst (mg)	Temperature (°C)	Time (min)	Yield (%)
1	EtOH/H_2O	10	80	15	71
2	EtOH/H_2O	20	80	15	82
3	EtOH/H_2O	30	80	15	74
4	EtOH/H_2O	40	80	15	74
5	**EtOH**	**20**	**80**	**15**	**90**
6	H_2O	20	80	15	76
7	Toluene	20	80	15	53
8	DMF	20	80	15	49
9	EtOH	20	60	15	72
10	EtOH	20	40	15	37
11	EtOH	20	rt	15	21
12	ETOH	10	80	15	73
13	ETOH	30	80	15	81
14	ETOH	40	80	15	83

Bold is to accentuate model reaction results.

Additionally, two additional reactions were performed under the optimal conditions as described below:

1. The synthesis of indazolophthalazinetriones carried out in the absence of Fe_3O_4@SiO_2@CPTMS@MBOL@Mn: reaction efficiency was very low (trace).
2. The reaction was done in the presence of (Fe_3O_4@SiO_2@CPTMS@MBOL) and no product was observed.
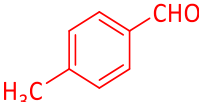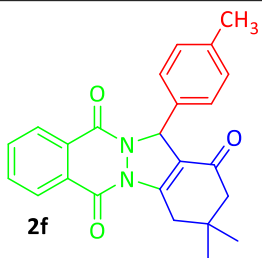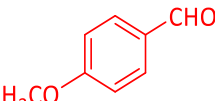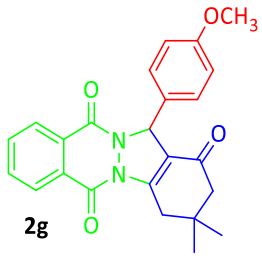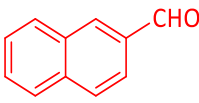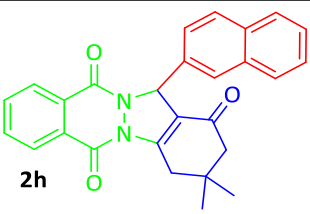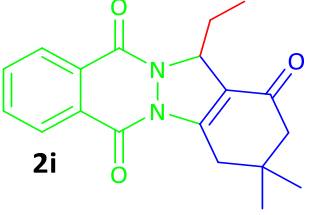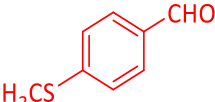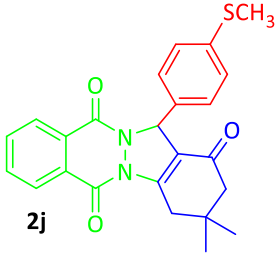
3.5. Synthesis of Diverse Indazolophthalazinetriones (**2a**–**j**)

According to the optimization of model reaction, different indazolophthalazinetriones (**2a**–**j**) were synthesized from the one-pot three-component condensation reaction of aldehydes, dimedone, and phthalhydrazide in EtOH under reflux conditions in attendance of the Mn-supported nano-catalyst with good to excellent yields in fast reaction times (Table 2).

Table 2. Synthesis of diverse indazolophthalazinetriones by the use of the Mn-supported nano-catalyst.
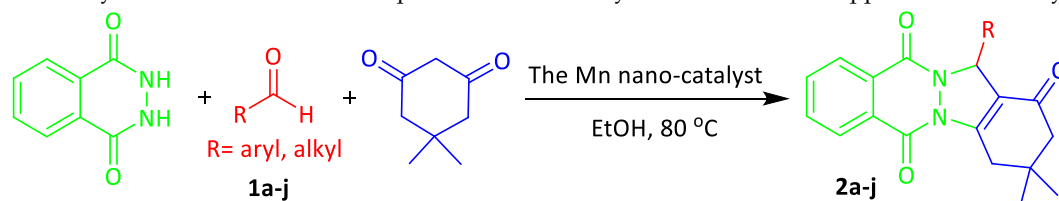
Entry	RCHO (1a-j)	Products (2a-j)	Time (min)	Yield %	M.P. °C, Found (Lit.) [37]
1	(1a)	2a	10	85	202–206 (206–208)
2	(1b)	2b	10	91	260–263 (262–264)
3	(1c)	2c	10	85	256–259 (258–260)
4	(1d)	2d	10	93	267–270 (269–271)
5	(1e)	2e	10	91	219–222 (219–221)

Table 2. *Cont.*

Entry	RCHO (1a-j)	Products (2a-j)	Time (min)	Yield %	M.P. °C, Found (Lit.) [37]
6	(1f)	2f	15	90	224–227 (226–228)
7	(1g)	2g	15	71	219–221 (220–221)
8	(1h)	2h	20	82	249–251 (251–252)
9	CH_3CH_2-CHO (1i)	2i	25	55	143–146 (145–147)
10	(1j)	2j	20	83	228–230 (229–231)

3.6. Characterization of the Products

All indazolophthalazinetriones were characterized and recognized by considering their physical and spectroscopic analysis and comparing to that reported in the literature. The structures of all the products were confirmed via their IR and NMR spectra (see Supplementary data).

3,3-Dimethyl-13-phenyl-3,4-dihydro-1*H*-indazolo[2,1,*b*]phthalazine-1,6,11(2*H*,13*H*)-trione (**2a**): mp 202–206 °C; FT-IR (KBr, cm^{-1}): The characteristic IR peaks: 3100, 3000, 2953, 1663; ^{1}H NMR (90 MHz, CDCl$_3$): δ_H = 7.80–8.37 (m, 4H), 7.26 (m, 5H), 6.45 (s, 1H), 3.30 (d, 2H, CH$_2$), 2.33 (s, 2H, CH$_2$), 1.22 (s, 6H, 2CH$_3$). ^{13}C NMR (75 MHz, CDCl$_3$): 28.7, 34.7, 38, 5, 65, 77.5, 118, 127, 127, 127.7, 128, 128.6, 128.7, 128.8, 128.9, 129, 133.5, 134.5, 136.3, 150.8, 154.2, 156, 192.

13-(4-Chlorophenyl)-3,3-dimethyl-3,4-dihydro-1*H*-indazolo[2,1-*b*]phthalazine-1,6,11(2*H*, 13*H*)-trione (**2b**): mp 260–263 °C; FT-IR (KBr, cm^{-1}): The characteristic IR peaks: 3100, 3000, 2957, 1660; ^{1}H NMR (90 MHz, CDCl$_3$): δ$_H$ = 7.81–8.41 (m, 4H), 7.32 (m, 4H), 6.41 (s, 1H), 3.30 (d, 2H, CH$_2$), 2.34 (s, 2H, CH$_2$), 1.21 (s, 6H, 2CH$_3$). ^{13}C NMR (75 MHz, CDCl$_3$): 28.5, 34.4, 38, 50, 61.3, 77, 118, 127.7, 128.2, 129.2, 134, 151, 154.3, 192.

13-(4-Bromophenyl)-3,3-dimethyl-3,4-dihydro-1*H*-indazolo[2,1-*b*]phthalazine-1,6,11(2*H*, 13*H*)-trione (**2c**): mp 256–259 °C; FT-IR (KBr, cm^{-1}): The characteristic IR peaks: 3100, 3000, *2959*, 1687, 1654; ^{1}H NMR (90 MHz, CDCl$_3$): δ$_H$ = 7.86–8.39 (m, 4H), 7.23–7.35 (m, 4H), 6.70 (s, 1H), 3.23–3.45 (d, 2H, CH$_2$), 2.34 (s, 2H, CH$_2$), 1.23 (s, 6H, 2CH$_3$).

3,3-Dimethyl-13-(3-nitrophenyl)-3,4-dihydro-1*H*-indazolo[2,1,*b*]phthalazine-1,6,11(2*H*,13*H*)-trione (**2d**): mp 267–270 °C; FT-IR (KBr, cm^{-1}): The characteristic IR peaks: 3100, 3000, 2962, 1661; ^{1}H NMR (300 MHz, CDCl$_3$): δ$_H$ = 7.87–8.40 (m, 4H), 6.52–7.59 (m, 4H), 6.52 (s, 1H), 3.24–3.47 (dd, 2H, CH$_2$), 2.35 (s, 2H, CH$_2$), 1.22 (s, 6H, 2CH$_3$). ^{13}C NMR (75 MHz, CDCl$_3$): 27.3, 28.4, 28.6, 34.7, 38, 50.8, 64, 76.5, 77, 117, 121.5, 123.7, 127.7, 128.2, 128.6, 129, 129.6, 134, 134.2, 134.7, 138.6, 148.5, 151.8, 154.6, 156, 192.

13-(2,4-Dichlorophenyl)-3,3-dimethyl-3,4-dihydro-1*H*-indazolo[2,1-*b*]phthalazine-1,6,11-(2*H*, 13*H*)-trione (**2e**): mp 219–222 °C; FT-IR (KBr, cm^{-1}): The characteristic IR peaks: 3100, 3000, 2964, 2940, 1663; ^{1}H NMR (90 MHz, CDCl$_3$): δ$_H$ = 7.75–8.38 (m, 4H), 7.13–7.26 (m, 3H), 6.6 (s, 1H), 3.3 (d, 2H, CH$_2$), 2.33 (s, 2H, CH$_2$), 1.22 (s, 6H, 2CH$_3$). ^{13}C NMR (75 MHz, CDCl$_3$): 28.8, 34.6, 38, 50.8, 63.5, 77, 127.6, 127.7, 128, 128.6, 129, 130.4, 131.7, 133.2, 133.7, 134.6, 135, 152, 154.3, 156, 192.

3,4-Dihydro-3,3-dimethyl-13-(4-methylphenyl)-2*H*-indazolo[2,1-*b*]phthalazine-1,6,11(13H)-trione (**2f**): mp 224–227 °C; FT-IR (KBr, cm^{-1}): The characteristic IR peaks: 3100, 3000, 2924, 1687, 1655; 1H NMR (90 MHz, CDCl$_3$): δ$_H$ = 7.77–8.28 (m, 4H), 7.17–7.35 (m, 4H), 6.4 (s, 1H), 3.3 (d, 2H, CH$_2$), 2.29–2.32 (m, 5H), 1.21 (s, 6H, 2CH$_3$).

13-(4-Methoxyphenyl)-3,3-dimethyl-3,4-dihydro-1*H*-indazolo[2,1-*b*]phthalazine-1,6,11-(2*H*, 13*H*)-trione (**2g**): mp 219–221 °C; FT-IR (KBr, cm^{-1}): The characteristic IR peaks: 3100, 3000, 2956, 1664; ^{1}H NMR (90 MHz, CDCl$_3$): δ$_H$ = 7.92–8.24 (m, 4H), 7.54–7.82 (m, 4H), 6.5 (s, 1H), 3.77 (s, OCH$_3$) 3.33 (d, 2H, CH$_2$), 2.33 (s, 2H, CH$_2$), 1.2 (s, 6H, 2CH$_3$).

3,4-Dihydro-3,3-dimethyl-13-(2-eylnaphtalene)-2*H*-indazolo[2,1-*b*]phthalazine-1,6,11(13*H*)-trione (**2h**): mp 249–251 °C; FT-IR (KBr, cm^{-1}): The characteristic IR peaks: 3100, 3000, 2967, 1681, 1664; ^{1}H NMR (90 MHz, CDCl$_3$): δ$_H$ = 7.45–8.38 (m, 11H), 6.62 (s, 1H), 3.24–3.5 (dd, 2H), 2.33 (s, 2H), 1.22(s, 6H). ^{13}C NMR (75 MHz, CDCl$_3$): 118.6, 124, 126.2, 126.3, 126.8, 127.7, 128, 128.2, 128.7, 129, 133.2, 133.4, 133.5, 133.6, 134.5, 150.8, 156, 192.

13-Ethyl-3,3-dimethyl-3,4-dihydro-1*H*-indazolo[2,1-*b*]phthalazine-1,6,11(2*H*,13*H*)-trione (**2i**): mp 264–267 °C; FT-IR (KBr, cm^{-1}): The characteristic IR peaks: 3100, 3000, 2962, 2931, 1652; ^{1}H NMR (90 MHz, CDCl$_3$): δ$_H$ = 7.81–8.35 (m, 4H), 5.69 (m, 1H), 3.16 (d, 2H, CH$_2$), 2.16–2.37 (m, 4H, 2CH$_2$), 1.19 (s, 6H, 2CH$_3$), 0.65–0.82 (t, 3H, CH$_3$).

3,4-Dihydro-3,3-dimethyl-13-(4-thiomethylphenyl)-2*H*-indazolo[2,1-*b*]phthalazine-1,6,11 (13*H*)-trione (**2j**): mp 228–230 °C; FT-IR (KBr, cm^{-1}): The characteristic IR peaks: 3100, 3000, 2959, 2978, 1663; ^{1}H NMR (90 MHz, CDCl$_3$): δ$_H$ = 7.84–8.37 (m, 4H), 7.1–7.35 (m, 4H), 6.4 (s, 1H), 3.21–3.45 (d, 2H, CH$_2$), 2.42 (s, 3H), 2.34 (s, 2H), 1.2 (s, 6H).

3.7. The Plausible Mechanism

A persuasive mechanism for the synthesis of diverse phthalazine-triones is illustrated below. The reaction was followed by the mixture of reagents in EtOH under reflux conditions in the presence of the Mn-supported nano-catalyst (Scheme 3).
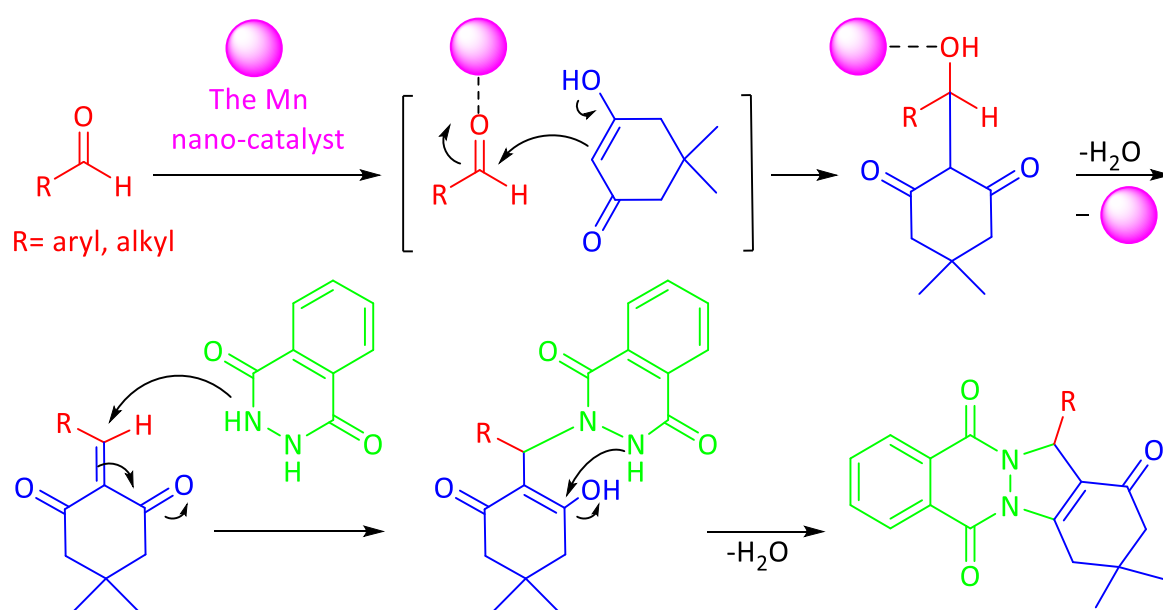
Scheme 3. Suggested mechanism for the synthesis of indazolophthalazinetrione.

The suggested mechanism is presumably in accordance with the Lewis acidity property of the Mn-supported nano-catalyst by connecting to the carbonyl group to simplify the nucleophilic attack of the enolic form of dimedone (Knoevenagel condensation) to aldehyde to form the intermediate with the subsequent deletion of water, the nucleophilic attack of phthalhydrazide, deletion of water, and the final cyclization to obtain the product [8,20].

3.8. Comparison of Catalytic Activity

Table 3 shows the comparison of the previous procedures (entries 1–9) in synthesis of 3,4-Dihydro-3,3-dimethyl-13-(4-methylphenyl)-2*H*-indazolo[2,1-*b*]phthalazine-1,6,11(13H)-trione with our present work (entry 10). In general, each procedure included some advantages. Through focusing on the previous studies, we could declare that this method accelerated the process of reaction and would be useful and efficient as well.

Table 3. Comparison of the Mn-supported nano-catalyst capability with the other catalysts in synthesis of 3,4-dihydro-3,3-mimethyl-13-(4-methylphenyl)-2*H*-indazolo[2,1-*b*]phthalazine-1,6,11(13H)-trione.

Refs.	Yield (%)	Time (min)	T [b] (°C)	Solvent [a]	Catalyst	Entry
[38]	90	40	70	SF	MNPs-guanidine (0.03 g)	1
[39]	86	30	80	H_2O	β-Cyclodextrin	2
[40]	66	60	100	SF	[Simp]$_3$PW$_{12}$O$_{40}$ (0.03 g)	3
[41]	70	60	100	SF	PTA@Fe$_3$O$_4$/EN-MIL-101 (0.02 g)	4
[42]	86	40	100	SF	Fe$_3$O$_4$@Silica sulfuric acid (0.075 g)	5
[43]	90	30	100	SF	MNPs-PSA (0.03)	6
[44]	86	30	Reflux	EtOH	H_2SO_4 (0.015 %mmole) in EtOH/H_2O	7
[45]	87	30	80	SF	MnFe2O4@SiO2@NH-NH2-PTA (0.03 g)	8
[46]	94	150	50	PEG	CAN (5 %mol)	9
PW [c]	90	15	Reflux	EtOH	Fe$_3$O$_4$@SiO$_2$@CPTMS@MBOL@Mn (0.02 g)	10

[a] SF = Solvent-free, [b] T = temperature, [c] PW = present work.

3.9. Reusability of the Mn-Supported Nano-Catalyst

To investigate the recyclability of the Mn-supported nano-catalyst for environmental and commercial applications, it was tested with the model reaction and found to be relatively capable even after five runs, and its activity was almost similar to that of the fresh one (90, 90, 88, 87, and 84%, respectively) (Figure 9). The stability of the Mn-supported nano-catalyst even after the fifth run was inspected by FT-IR and SEM techniques (Figures 10 and 11). As can be observed, even after consecutive 5 runs there were no significant changes in the IR spectrum, and the grey sintered shape of nano-catalyst was also preserved regularly.
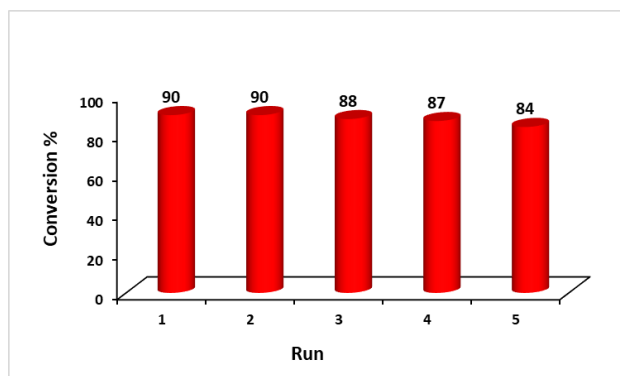

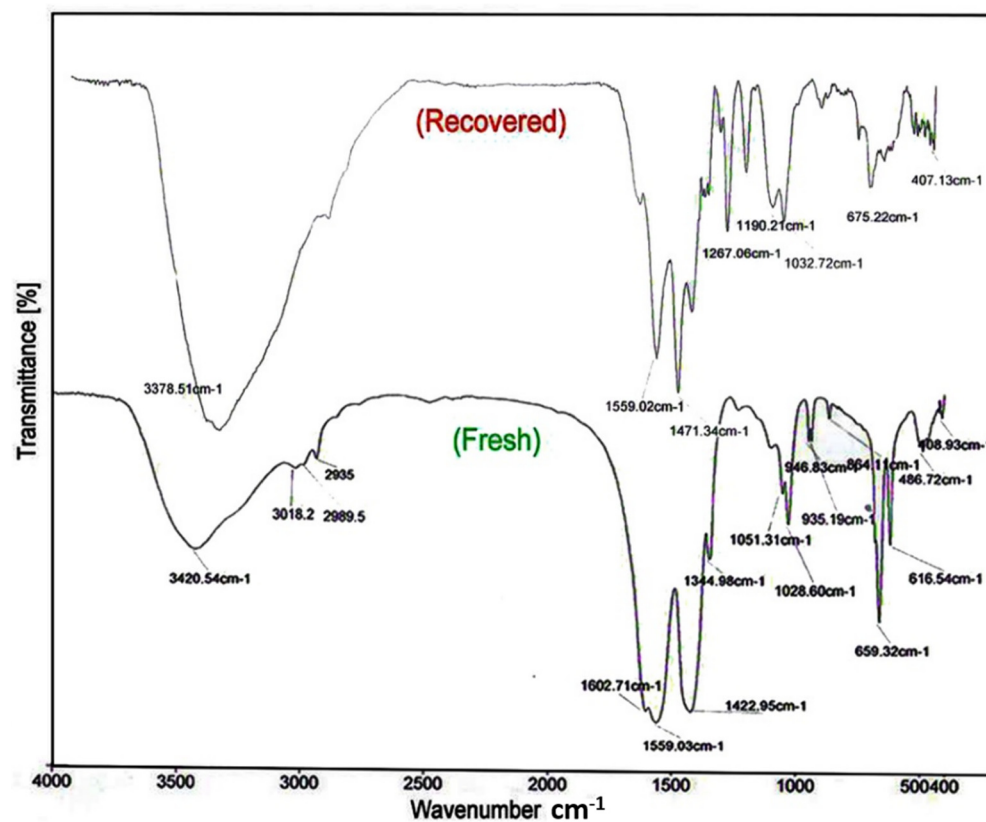**Figure 9.** Reusability of the Mn-supported nano-catalyst.

Figure 10. FT-IR spectra of fresh and recovered Mn-supported nano-catalysts.
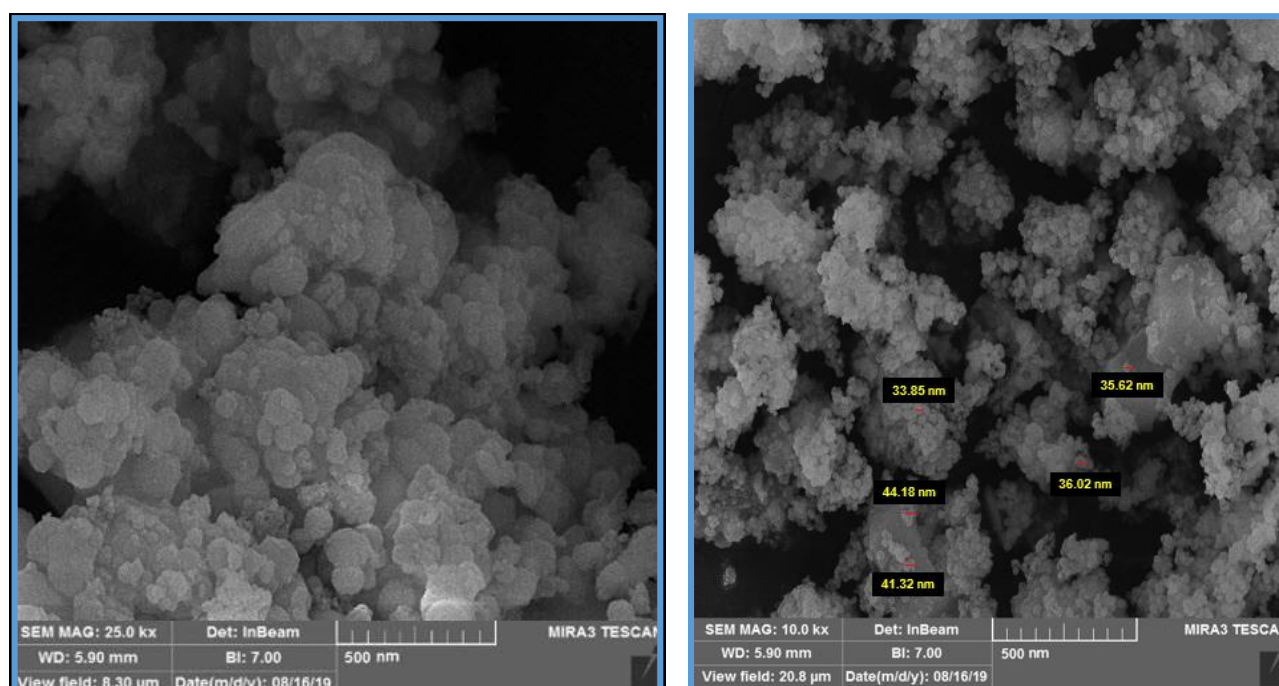
Figure 11. SEM image of recovered Mn-supported nano-catalyst.

3.10. Antibacterial Properties

The antibacterial properties of the Mn-supported nano-catalyst were studied against a number of gram-positive and gram-negative bacterial strains, and DMSO was used as a blank (Table 4). The catalyst inhibited the growth of bacterial strains, producing a zone of inhibition of diameter 5–30 mm. The Mn-supported nano-catalyst was even more effective against Serratia marcescens in gram-negative bacteria than the standard tetracycline antibiotic. Since the comparison of the size of inhibition zones is generally not reliable, the MIC value of the compound was also determined. The results indicated that the MIC value of the Mn-supported nano-catalyst against the tested organisms was about 8 mg/mL. The MIC value of a standard tetracycline antibiotic is about 8 mg/mL.

Table 4. Antibacterial activity of Mn-supported nano-catalyst that was expressed as diameter of inhabitation zone (mm) and minimum inhibitory concentration (MIC).

Microorganisms	Standard	Blank	Zone of Inhabitation (mm)
	Tetracycline (10 mg/mL)	DMSO	the Mn catalyst
MIC (mg/mL)	8	-	8
Gram (+)			
Bacillus thuringiensis	30	-	10
Bacillus cereus	36	-	20
Staphylococcus aureus	30	-	5
Gram (−)	25	-	20
Pseudomonas aeruginosa			
Serratia marcescens	20	-	30
Escherichia coli	22	-	15
Klebsiella pneumoniae	25	-	5

4. Conclusions

In conclusion, we demonstrated the preparation of an appropriate Mn nano-catalyst supported on magnetic iron oxide and functionalized with mercaptobenzoxazole. To investigate the application of the nano-catalyst, it was used for synthesis of diverse In-

dazolophthalazinetriones through the one-pot three-component condensation reaction of aldehydes, dimedone, and phthalhydrazide in ethanol under reflux conditions. The reactions developed with good yields and short times. In fact, the Lewis acidity property of the Mn catalyst caused the connection with the carbonyl group of different aldehyde derivates to accelerate the nucleophilic attack of dimedone to generate the intermediates for the formation of final products. Additionally, we studied the antibacterial properties of the catalyst against a number of gram-positive and gram-negative bacterial strains and determined that the nano-catalyst would be more effective against Serratia marcescens in gram-negative bacteria than the standard tetracycline antibiotic. Furthermore, we investigated the reusability of the Mn-catalyst and revealed that the catalyst could be reused for five runs without any significant loss in catalytic activity. According to a comparison with several similar projects, we could declare that the represented catalyst has a reasonable ability to proceed the mentioned chemical reactions.

Supplementary Materials: The supplementary date are available online at https://www.mdpi.com/article/10.3390/chemistry3030056/s1.

Author Contributions: M.A.: investigation, formal analysis, methodology, and writing original draft preparation. D.H.: conceptualization, supervision, project administration, review and editing. S.H.: conceptualization, data curation, V.K.: conceptualization, methodology. All authors have read and agreed to the published version of the manuscript.

Data Availability Statement: Data from experiments can be accessed from supplementary information.

Conflicts of Interest: The authors declare no conflict of interest.

References

1. Al-Assar, F.; Zelenin, K.N.; Lesiovskaya, E.E.; Bezhan, I.P.; Chakchir, B.A. Synthesis and Pharmacological Activity of 1-Hydroxy-, 1-Amino-, and 1-Hydrazino-Substituted 2,3-Dihydro-1H-pyrazolo[1,2-a]pyridazine-5,8-diones and 2,3-Dihydro-1H-pyrazolo[1,2-b]phthalazine-5,10-diones. *Pharm. Chem. J.* **2002**, *36*, 598–603. [CrossRef]
2. Ryu, C.K.; Park, R.E.; Ma, M.Y.; Nho, J.H. Synthesis and antifungal activity of 6-arylamino-phthalazine-5,8-diones and 6,7-bis(arylthio)-phthalazine-5,8-diones. *Bioorg. Med. Chem. Lett.* **2007**, *17*, 2577–2580. [CrossRef] [PubMed]
3. Sinkkonen, J.; Ovcharenko, V.; Zelenin, K.N.; Bezhan, I.P.; Chakchir, B.A.; Al-Assar, F.; Pihlaja, K. 1H and 13C NMR Study of 1-Hydrazino-2,3-dihydro-1H-pyrazolo[1,2-a]pyridazine-5,8-diones and -1H-pyrazolo[1,2-b]phthalazine-5,10-diones and Their Ring-Chain Tautomerism. *Eur. J. Org. Chem.* **2002**, *13*, 2046. [CrossRef]
4. Zhang, L.; Guan, L.P.; Sun, X.Y.; Wei, C.X.; Chai, K.Y.; Quan, Z.S. Synthesis and Anticonvulsant Activity of 6-Alkoxy-[1,2,4]Triazolo[3,4-*a*]Phthalazines. *Chem. Biol. Drug Des.* **2009**, *73*, 313–319. [CrossRef] [PubMed]
5. Li, J.; Zhao, Y.F.; Yuan, X.Y.; Xu, J.X.; Gong, P. Synthesis and Anticancer Activities of Novel 1,4-Disubstituted Phthalazines. *Molecules* **2006**, *11*, 574–582. [CrossRef] [PubMed]
6. Nomoto, Y.; Obase, H.; Takai, H.; Teranishi, M.; Nakamura, J.; Kubo, K. Studies on Cardiotonic Agents. II.: Synthesis of Novel Phthalazine and 1, 2, 3-Benzotriazine Derivatives. *Chem. Pharm. Bull.* **1990**, *38*, 2179–2183. [CrossRef]
7. Xu, Y.; Guo, Q.X. Syntheses of Heterocyclic Compounds under Microwave Irradiation. *Heterocycles* **2004**, *63*, 903–974. [CrossRef]
8. Karunaratne, C.V.; Sarkisian, R.G.; Reeves, J.; Deng, Y.; Wheeler, K.A.; Wang, H. Multicomponent Reaction through Cooperative Trio Catalysis Incorporating Enamine, BrønstedAcid and Metal Lewis Acid Catalysis: A Concise Route to Access Chromans. *Org. Biomol. Chem.* **2017**, *15*, 4933–4936. [CrossRef] [PubMed]
9. Kumar, A.; Maurya, R.A. Synthesis of polyhydroquinoline derivatives through unsymmetric Hantzsch reaction using organocatalysts. *Tetrahedron* **2007**, *63*, 1946–1952. [CrossRef]
10. Bhaskaruni, S.V.; Maddila, S.; Gangu, K.K.; Jonnalagadda, S.B. A Review on multi-component green synthesis of N-containing heterocycles using mixed oxides as heterogeneous catalysts. *Arab. J. Chem.* **2020**, *13*, 1142–1178. [CrossRef]
11. Chen, M.N.; Mo, L.P.; Cui, Z.S.; Zhang, Z.H. Magnetic nanocatalysts: Synthesis and application in multicomponent reactions. *Curr. Opin. Green Sustain. Chem.* **2019**, *15*, 27–37. [CrossRef]
12. Sayyafi, M.; Seyyedhamzeh, M.; Khavasi, H.R.; Bazgir, A. One-pot, three-component route to 2H-indazolo [2, 1-b] phthalazine-triones. *Tetrahedron* **2008**, *64*, 2375–2378. [CrossRef]
13. Shekouhy, M.; Hasaninejad, A. Ultrasound-promoted catalyst-free one-pot four component synthesis of 2H-indazolo [2, 1-b] phthalazine-triones in neutral ionic liquid 1-butyl-3-methylimidazolium bromide. *Ultrason. Sonochem.* **2012**, *19*, 307–313. [CrossRef] [PubMed]

14. Abbasi, M.; Nazifi, S.M.R.; Nazifi, Z.S.; Massah, A.R. Synthesis, characterization and in vitro antibacterial activity of novel phthalazine sulfonamide derivatives. *J. Chem. Sci.* **2017**, *129*, 1257–1266. [CrossRef]

15. Kiasat, R.; Mouradezadegun, A.; Saghanezhad, J. Phospho sulfonic acid: A novel and efficient solid acid catalyst for the one-pot preparation of 2H-indazolo [2, 1-b]-phthalazine-triones. *J. Serbian Chem. Soc.* **2013**, *78*, 469–476. [CrossRef]

16. Albadi, J.; Jalali, M.; Momeni, A. Cobalt-based nanocatalyst catalyzed one-pot four-component synthesis 2H-indazolo [2, 1-b] phthalazine-triones under solvent-free condition. *Res. Chem. Intermed.* **2018**, *44*, 2395–2404. [CrossRef]

17. Nikzad Shalkouhi, S.; Kefayati, H.; Shariati, S. Synthesis, characterization and catalytic application of Fe$_3$O$_4$@ Cys–SO$_3$H for preparation of 2H-indazolo [1, 2-b] phthalazine-triones. *Iran.J. Catal.* **2018**, *8*, 213–220.

18. Mousapour, M.; Shirini, F.; Abedini, M. Efficient Synthesis of 2 H-Indazolo [2, 1-b] Phthalazine-Triones Using [PVPH] ClO$_4$ as a Modified Polymeric Catalyst. *Polycycl. Aromt. Compd.* **2019**, *41*, 1–8. [CrossRef]

19. Sabitha, G.; Srinivas, C.; Raghavendar, A.; Yadav, J.S. Phosphomolybdic Acid (PMA)–SiO$_2$ as a Heterogeneous Solid Acid Catalyst for the One-Pot Synthesis of 2H-Indazolo [1, 2-b] phthalazine-triones. *Helv. Chim. Acta.* **2010**, *93*, 1375–1380. [CrossRef]

20. Doustkhah, E.; Rostamnia, S. Covalently bonded sulfonic acid magnetic graphene oxide: Fe$_3$O$_4$@ GO-Pr-SO$_3$H as a powerful hybrid catalyst for synthesis of indazolophthalazinetriones. *J. Colloid Interface Sci.* **2016**, *478*, 280–287. [CrossRef] [PubMed]

21. Nagarapu, L.; Bantu, R.; Mereyala, H.B. TMSCl-mediated one-pot, three-component synthesis of 2H-indazolo [2, 1-b] phthalazine-triones. *J. Heterocycl. Chem.* **2009**, *46*, 728–731. [CrossRef]

22. Varghese, A.; Nizam, A.; Kulkarni, R.; Georg, L. Solvent-free synthesis of 2H-indazolo [2, 1-b] phthalazine-triones promoted by cavitational phenomenon using iodine as catalyst. *Eur. J. Chem.* **2013**, *4*, 132–137. [CrossRef]

23. Mosaddegh, E.; Hassankhani, A. A rapid, one-pot, four-component route to 2H-indazolo [2, 1-b] phthalazine-triones. *Tetrahedron Lett.* **2011**, *52*, 488–490. [CrossRef]

24. Abedini, M.; Shirini, F.; Mousapour, M. Poly (vinylpyrrolidinium) perchlorate as a new and efficient catalyst for the promotion of the synthesis of polyhydroquinoline derivatives via Hantzsch condensation. *Res. Chem. Intermed.* **2016**, *42*, 2303–2315. [CrossRef]

25. Teimuri-Mofrad, R.; Esmati, S.; Rabiei, M.; Gholamhosseini-Nazari, M. Efficient synthesis of new pyrano [3, 2-b] pyran derivatives via Fe$_3$O$_4$@ SiO$_2$-IL-Fc catalyzed three-component reaction. *Heterocycl. Comm.* **2017**, *23*, 439–444. [CrossRef]

26. Kaur, P.; Hupp, J.T.; Nguyen, S.T. Porous organic polymers in catalysis: Opportunities and challenges. *ACS Catal.* **2011**, *1*, 819–835. [CrossRef]

27. Zhang, Y.; Riduan, S.N. Functional porous organic polymers for heterogeneous catalysis. *Chem. Soc. Rev.* **2012**, *41*, 2083–2094. [CrossRef] [PubMed]

28. Polshettiwar, V.; Luque, R.; Fihri, A.; Zhu, H.; Basset, M.B. Magnetically recoverable nanocatalysts. *Chem. Rev.* **2011**, *111*, 3036–3075. [CrossRef] [PubMed]

29. Wang, R.; Wang, X.; Xi, X.; Hu, R.; Jiang, G. Preparation and photocatalytic activity of magnetic Fe$_3$O$_4$/SiO$_2$/TiO$_2$ composites. *Adv. Mater. Sci. Eng.* **2012**, *2012*. [CrossRef]

30. Jahanshahi, P.; Mamaghani, M. Efficient and straightforward access to diverse and densely functionalized chromenes by 3-amino-1, 2, 4-triazole supported on hydroxyapatite-encapsulated-γ-Fe$_2$O$_3$ (γ-Fe$_2$O$_3$@ HAp@ CPTMS@AT) as a new magnetic basic nanocatalyst. *React. Kinet. Mech. Catal.* **2020**, *130*, 955–977. [CrossRef]

31. Stebounova, L.V.; Gonzalez-Pech, N.I.; Peters, T.M.; Grassian, V.H. Physicochemical properties of air discharge-generated manganese oxide nanoparticles: Comparison to welding fumes. *J. Environ. Sci.* **2018**, *5*, 696–707. [CrossRef]

32. Nasrollahzadeh, M.; Issaabadi, Z.; Sajadi, S.M. Fe$_3$O$_4$@ SiO$_2$ nanoparticle supported ionic liquid for green synthesis of antibacterially active 1-carbamoyl-1-phenylureas in water. *RSC Adv.* **2018**, *8*, 27631–27644. [CrossRef]

33. Malek, T.J.; Chaki, S.H.; Tailor, J.P.; Deshpande, M.P. Nonisothermal decomposition kinetics of pure and Mn-doped Fe$_3$O$_4$ nanoparticles. *J. Therm. Anal. Calorim.* **2018**, *132*, 895–905. [CrossRef]

34. Jiang, Z.; Huang, K.; Yang, D.; Wang, S.; Zhong, H.; Jiang, C. Facile preparation of Mn$_3$O$_4$ hollow microspheres via reduction of pentachloropyridine and their performance in lithium-ion batteries. *RSC Adv.* **2017**, *7*, 8264–8271. [CrossRef]

35. Habibi, D.; Heydari, S.; Afsharfarnia, M.; Rostami, Z. A versatile synthesis of arylaminotetrazoles by a magnetic Fe@ Phendiol@ Mn nano-particle catalyst and its theoretical studies. *Appl. Organomet. Chem.* **2017**, *31*, e3826. [CrossRef]

36. Ariannezhad, M.; Habibi, D.; Heydari, S. Copper nanoparticles: A capable and versatile catalyst for the synthesis of diverse 1-phenyl-1H-tetrazoles from amino acids. *Polyhedron* **2019**, *160*, 170–179. [CrossRef]

37. Atashkar, B.; Rostami, A.; Gholami, H.; Tahmasbi, B. Magnetic nanoparticles Fe$_3$O$_4$-supported guanidine as an efficient nanocatalyst for the synthesis of 2H-indazolo [2, 1-b] phthalazine-triones under solvent-free conditions. *Res. Chem. Intermed.* **2015**, *41*, 3675–3681. [CrossRef]

38. Chate, A.V.; Bhadke, P.K.; Khande, M.A.; Sangshetti, J.N.; Gill, C.H. β-cyclodextrin as a supramolecular catalyst for the synthesis of 2H-indazolo [2, 1-b] phthalazine-trione derivatives in water and their antimicrobial activities. *Chin. Chem. Lett.* **2017**, *28*, 1577–1582. [CrossRef]

39. Tayebee, R.; Abdizadeh, M.F.; Maleki, B.; Shahri, E. Heteropolyacid-based ionic liquid [Simp]$_3$PW$_{12}$O$_{40}$ nanoparticle as a productive catalyst for the one-pot synthesis of 2H-indazolo [2, 1-b] phthalazine-triones under solvent-free conditions. *J. Mol. Liq.* **2017**, *241*, 447–455. [CrossRef]

40. Hashemzadeh, A.; Amini, M.M.; Tayebee, R.; Sadeghian, A.; Durndell, L.J.; Isaacs, M.A.; Lee, A.F. A magnetically-separable H3PW$_{12}$O$_{40}$@ Fe$_3$O$_4$/EN-MIL-101 catalyst for the one-pot solventless synthesis of 2H-indazolo [2, 1-b] phthalazine-triones. *Mol. Catal.* **2017**, *440*, 96–106. [CrossRef]

41. Kiasat, A.R.; Davarpanah, J. Fe$_3$O$_4$@ silica sulfuric acid nanoparticles: An efficient reusable nanomagnetic catalyst as potent solid acid for one-pot solvent-free synthesis of indazolo [2, 1-b] phthalazine-triones and pyrazolo [1, 2-b] phthalazine-diones. *J. Mol. Catal. A Chem.* **2013**, *373*, 46–54. [CrossRef]

42. Rostami, A.; Tahmasbi, B.; Yari, A. Magnetic nanoparticle immobilized N-propylsulfamic acid as a recyclable and efficient nanocatalyst for the synthesis of 2H-indazolo [2, 1-b] phthalazine-triones in solvent-free conditions: Comparison with sulfamic acid. *Bull. Korean Chem. Soc.* **2013**, *34*, 1521–1524. [CrossRef]

43. Khurana, J.M.; Magoo, D. Efficient one-pot syntheses of 2H-indazolo [2, 1-b] phthalazine-triones by catalytic H$_2$SO$_4$ in water–ethanol or ionic liquid. *Tetrahedron Lett.* **2009**, *50*, 7300–7303. [CrossRef]

44. Mozafari, R.; Heidarizadeh, F. Phosphotungstic acid supported on SiO$_2$@ NHPhNH2 functionalized nanoparticles of MnFe$_2$O$_4$ as a recyclable catalyst for the preparation of tetrahydrobenzo [b] pyran and indazolo [2, 1-b] phthalazine-triones. *Polyhedron* **2019**, *162*, 263–276. [CrossRef]

45. Mazaahir, K.; Ritika, C.; Anwar, J. Efficient CAN catalyzed synthesis of 1H-indazolo [1, 2-b] phthalazine-1, 6, 11-triones: An eco-friendly protocol. *Chin. Sci. Bull.* **2012**, *57*, 2273–2279. [CrossRef]

46. Abedini, M.; Shirin, F.; Mohammad-Alinejad Omran, J. Efficient synthesis of 2H-indazolo [2, 1-b] phthalazine-trione derivatives using succinimidinium N-sulfonic acid hydrogen sulfate as a new ionic liquid catalyst. *J. Mol. Liq.* **2015**, *212*, 405–412. [CrossRef]